Low-mass dileptons at 200 GeV/nucleon

J. Murray and W. Bauer
National Superconducting Cyclotron Laboratory, Michigan State University, East Lansing, Michigan 48824

K. Haglin
Department of Physics, Lawrence University, Appleton, Wisconsin 54912
(Received 31 October 1996; revised manuscript received 10 October 1997)

We use a simple QCD-based model to study particle production in S+Au collisions at 200 GeV/nucleon. A requisite consistency is met for the hadronic observables (π^0 and π^- spectra) while pursuing estimates for e^+e^- production. Since radiative decays of initially produced hadrons has accounted for only a portion of the observed dileptons at the CERN SPS, we search for additional mechanisms. By including contributions from prompt secondary hadronic scatterings, $\pi\rho\rightarrow\pi e^+e^-$, and adding to $\pi^+\pi^-$ annihilation and hadronic decays, part of the ''excess'' dilepton signal can possibly be interpreted. [S0556-2813(98)03202-6]

PACS number(s): 25.75.−q, 12.38.Mh, 24.85.+p, 24.10.Lx

I. INTRODUCTION

Measuring and analyzing electromagnetic radiation from heavy-ion collisions represents a significant experimental challenge compared to hadronic signals owing to the relatively small cross sections. The additional information they provide certainly justifies the undertaking. Hadrons produced in the initial stages of the collision interact on average several times before leaving the reaction zone. Consequently, any information embedded in hadronic dynamics is completely masked by multiple scatterings. Dileptons are not disturbed by the hadronic environment even though they are produced at all stages of the collisions as they have long mean free paths. They are dubbed ''clean probes'' of the collision dynamics.

Recent results from CERN [1] have brought about a surge of activity in search of quantitative interpretation. The proton-induced reactions (p+Be and p+Au at 450 GeV) are consistent with predictions from primary particle production and subsequent radiative and/or Dalitz decays suggesting that the e^+e^- yields are fairly well understood. Yet, the heavy-ion data (S+Au at 200 GeV/nucleon) show a significant excess as compared to the same model for meson production and electromagnetic decays. When integrated over pair invariant mass up to 1.5 GeV, the number of electron pairs exceeded the ''cocktail'' prediction by a factor of 5 ± 2. It is clear that two-pion annihilation contributes in the heavy-ion reactions as fireball-like features emerge and support copious pion production [2]. Vector dominance arguments would naturally lead to extra production around the rho mass. Yet, the excess is most pronounced between the two-pion threshold and the rho mass.

The nature of the enhancement suggests several possibilities. Medium modifications resulting in a shifted rho mass could be responsible [3]. Along these lines, consequences arising from a modified pion dispersion relation have been investigated considering finite temperature effects [4] and collisions with nucleons and Δ resonances [5]. Enhanced η' production, as suggested in Ref. [6], seems to be ruled out by inclusive photon measurements [7,8].

Secondary scattering of pions and other resonances has also been studied [9] focusing on the role of the a_1 through $\pi\rho\rightarrow a_1\rightarrow\pi e^+e^-$. The contribution was shown to be relevant but not sufficient for interpreting the data. We extend the secondary scattering investigation in the present calculation by including nonresonance dilepton-producing $\pi\rho\rightarrow\pi e^+e^-$ reactions [10]. We shall organize our paper in the following way. In Sec. II we discuss the event generator providing the basis of the reaction description and we compare to pion spectra from experiment. Then in Sec. III we introduce an algorithm for estimating secondary scattering. The prompt, or nonresonance, $\pi\rho\rightarrow\pi e^+e^-$ reactions are modeled with an effective field theory. A brief description of gauge-invariantly introducing strong-interaction form factors also appears. In Sec. IV we discuss normalization and acceptance effects, followed by the results and conclusions in Sec. V.

II. PRIMARY SCATTERING

Future collider energies, several thousand GeV per nucleon in the center of mass, probe distances much smaller than the nucleon. Models must of course incorporate QCD to describe the subnucleonic features. Quarks and gluons then comprise the appropriate degrees of freedom for a QCD transport theory. They are propagated through spacetime approximating the dynamics of collisions to be explored at RHIC and LHC [11–14]. Evolution continues until soft processes dominate and hadronization occurs.

Whether or not a quark-gluon plasma can be experimentally detected depends largely on the characteristics of the collision in its absence, something we shall call background. In order to better quantify this background, simulations without ''built-in'' plasma formation that still assume a QCD description of nucleon scattering must be explored. HIJING, developed by Wang and Gyulassy [15], is precisely this type of model and has been used to look at multiple minijet production, shadowing and jet quenching in pA and AA collisions.

The simulation we develop is similar to HIJING. It is based on a simple prescription that uses QCD to characterize the individual nucleon-nucleon collisions and uses Glauber-

type geometry to determine the scaling. The kinematics of the nucleon-nucleon collisions are handled by PYTHIA and JETSET [16], high energy event-generators using QCD matrix elements as well as the Lund fragmentation scheme. A somewhat detailed description of the model is outlined below.

Initialization of nucleons inside nuclei. The nucleons are positioned randomly inside each nucleus according to the size of the nucleus and are given random Fermi momentum in the x-y plane and are given z-momentum proportional to the lab energy (or center of mass energy).

Number of collisions. The number of collisions is determined geometrically [17]. For a proton-nucleus collision,

$$n(b)=\sigma_{NN}\int dx\ dy\ dz\ \rho(\sqrt{b^2+z^2}). \tag{2.1}$$

For nucleus-nucleus collisions,

$$N(b)=\sigma_{NN}\int dx\ dy\ dz_1\ dz_2 \times\rho_A(\sqrt{x^2+y^2+z_1{}^2})\rho_B(\sqrt{x^2+(y-b)^2+z_2{}^2}). \tag{2.2}$$

Picking scattering partners. Two nucleons are chosen at random from each nuclei and are allowed to scatter when, and if, they meet several criteria: First, the two nucleons cannot have scattered previously. Second, the nucleons must be within one cross-sectional radius of one another in the transverse beam direction,

$$\sqrt{(x_t-x_p)^2+(y_t-y_p)^2}\leqslant\sqrt{\sigma_{NN}/\pi}. \tag{2.3}$$

Thirdly, the center of mass energy, $\sqrt{s}$, must be above 6 GeV. This limit is chosen because it is on the order of the energy where perturbative QCD is no longer applicable. And lastly, if the reaction is proton-induced the pair must be moving toward one another in the transverse plane. If the two nucleons meet these criteria, they are allowed to scatter.

Scattering and rescattering. PYTHIA chooses partons to participate in the hard scattering from each nucleon. The partons that are chosen, as well as the momentum fraction they carry, are based on known parton distributions [18]. After the individual partons have had a hard scattering and are color connected with the diquarks from the remaining nucleon, strings are formed. The kinematics of the fragments from the string are determined by JETSET. Any partonic radiation that is not color connected to either string goes directly into the nucleus-nucleus final state. This string is then put back into the nuclei and allowed to rescatter as a ''wounded'' nucleon. The wounded nucleon has the string's momentum while its position is updated to halfway between the original nucleons' positions through,

$$(x_1,y_1)(x_2,y_2)\rightarrow\left(\frac{x_1+x_2}{2},\frac{y_1+y_2}{2}\right). \tag{2.4}$$

Final state. After all nucleons have experienced their geometrically determined number of collisions or they have center-of-mass energies below the cutoff, particles present in each nucleon's temporary array constitute the final state.

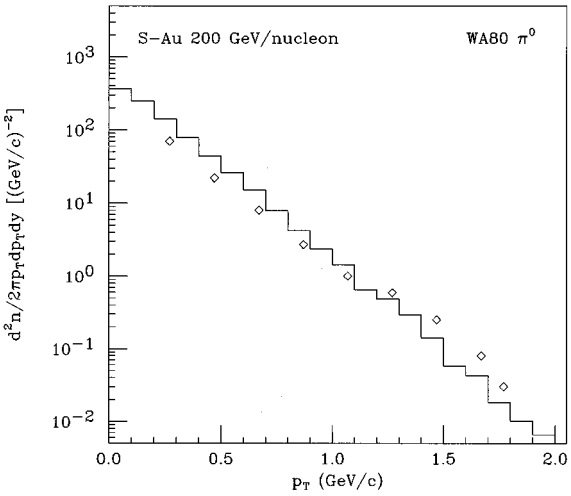

FIG. 1. π^0 p_T distribution from WA80 as compared with the model.

Hadronic observables from the model have been compared against data for several systems. Although the model is based on very simple premises, it reproduces the main features characterizing hadronic final states. Most notable for the present work, we have made comparisons to S+Au hadronic data as well as dilepton CERN SPS data (see Sec. V for dilepton data). Our model matches the π^0 spectrum from WA80 [19], as well as the π^-s from NA35 [20]. The two comparisons are shown in Figs. 1 and 2, respectively. The p_T distribution of neutral pions is slightly above the data at low p_T and slightly below the data for high p_T pions. This might account for part of the difference in kinematic acceptance discussed later in Sec. IV.

III. SECONDARY SCATTERING

Dileptons from pseudoscalars (π^0,η,η') and vectors (ω,ρ^0,ϕ) produced in the primary scattering phase are not enough to account for the S+Au data. Our model also incorporates secondary scattering of hadronic resonances. All π's

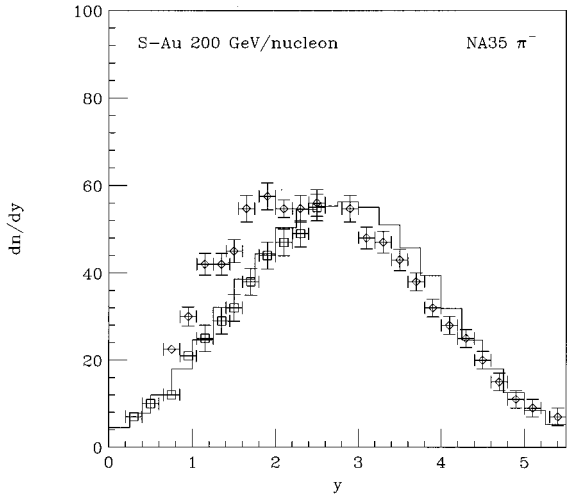

FIG. 2. π^- rapidity distribution from NA35 compared to the model.

and ρ's formed during the primary collisions of nucleons will have a chance to scatter amongst themselves before decaying. The reactions we consider are of two types, one which produces a resonance that decays to dileptons and the other which goes to dileptons directly.

Of the first type, $\pi^+\pi^-\to\rho^0\to e^+e^-$ and $\pi^0\rho^\pm\to a_1{}^\pm\to\pi^\pm e^+e^-$ have been included. To accomplish these types of scattering, pions and rhos must of course appear in the final state of the model described in the previous section. As the default, JETSET automatically decays all hadronic resonances, but it also contains provisions to prohibit them. We thus allow neutral pions to scatter from charged rhos when conditions are favorable. Technically, the steps involved in secondary scattering are similar to those for primary scattering.

Number of collisions. The number of collisions is again determined geometrically using the appropriate density and cross section.

Picking scattering partners. A $\pi^+\pi^-$ or $\pi\rho$ pair is randomly chosen and allowed to scatter if (1) the pair has not already scattered, and (2) the pair is within one cross-sectional radius of one another in the transverse beam direction. The cross section for creating a ρ^0 resonance is taken to be

$$\sigma(\sqrt{s})=\frac{\pi}{\boldsymbol{k}^2}\frac{{\Gamma_{\text{partial}}}^2}{(\sqrt{s}-m_{\text{res}})^2+{\Gamma_{\text{full}}}^2/4}, \tag{3.1}$$

with $\boldsymbol{k}$ being the center-of-mass momentum. The full and partial decay widths for $\rho^0\to\pi^+\pi^-$ are set to 152 MeV. The situation for creating an a_1 resonance through $\pi\rho$ scattering is handled somewhat differently than creating a ρ^0 through a $\pi^+\pi^-$ collision. Since our model scatters π's and ρ's resonantly and nonresonantly, the cross section used to determine whether or not a pair will scatter should be the total cross section. The total cross section for $\pi\rho$ scattering determines how many and how often the charged rhos scatter with pions. This way the pairs will be chosen according to the total cross section and the normalization of each type of scattering (resonant or nonresonant) will be determined by the branching ratios for each process. This normalization will be explained in greater detail later in the paper. Since data exists for $\pi\rho$ scattering [22,23], a parametrization can be used for the total cross section. Based on the general shape of the data, we use a simple Breit-Wigner shape for the function normalized by what the cross section should be near the a_1 peak. The resultant cross section is parametrized for $\sqrt{s}\geqslant 0.9$ GeV by

$$\sigma(\sqrt{s})=\frac{0.72\ \text{GeV}^2\ \text{mb}}{(\sqrt{s}-1.1\ \text{GeV})^2+\Gamma^2/4}. \tag{3.2}$$

Resonance formation and decay. The kinematics of the resonances are determined from the pair of hadrons while JETSET decays the resonance into dileptons using appropriate functions for $d\Gamma/dM^2$ and $|\mathcal{M}|^2$ resulting from analyses of an appropriate Lagrangian [21].

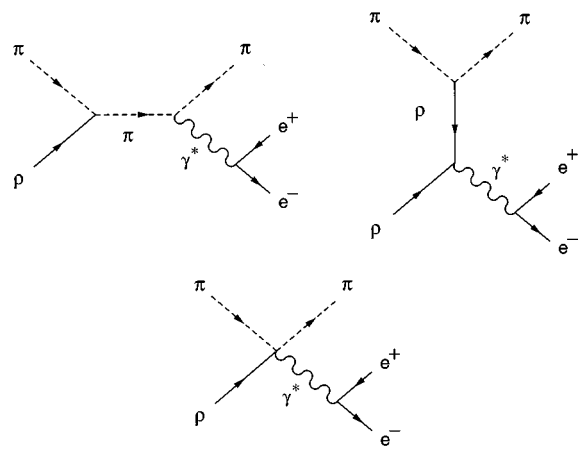

FIG. 3. Contributing Feynman diagrams for $\pi\rho\to\pi e^+e^-$.

Dileptons from secondary scatterings of the resonance-type increase the number significantly in the region around the ρ^0 mass, but not in the region with the largest gap, $0.2\ \text{GeV}\leqslant M^2\leqslant 0.5\ \text{GeV}$.

The nonresonant component is estimated here by computing the sole process $\pi^0\rho^\pm\to\pi^\pm e^+e^-$. The other $\pi\rho$ channels that contribute to dilepton production involve Feynman graphs that result in a singularity and must be regulated in a full T-matrix or some other effective approach [24]. Real photon studies [25,35,33] suggest that contributions from $\pi^\pm\rho^0\to\pi^\pm e^+e^-$ and $\pi^\mp\rho^\pm\to\pi^0e^+e^-$ are comparable to the process we calculated. Therefore we have assumed the same cross section and dilepton mass dependence for the other isospin channels not calculated in this paper. To this level of estimate, isospin averaging and ignoring interference effects between these and the resonant a_1 contributions is not worrisome. The prescription for directly scattering pions and rhos is very similar to the one used for resonance scattering as detailed below.

Picking scattering partners. The same prescription used for creating an a_1 resonance described previously is also used for picking scattering pairs in nonresonant scattering.

Scattering. Since this is a nonresonant process, the Monte Carlo procedure directly determines the kinematics of the final state. Necessary ingredients for such procedures include an interaction Lagrangian and a resulting squared matrix element. The Lagrangian employed is [25]

$$\mathcal{L}=|D_\mu\Phi|^2-{m_\pi}^2|\Phi|^2-\frac{1}{4}|\rho_{\mu\nu}|^2+\frac{1}{2}{m_\rho}^2|\rho_\mu|^2-\frac{1}{4}F_{\mu\nu}F^{\mu\nu}, \tag{3.3}$$

where $D_\mu=\partial_\mu-ieA_\mu-ig_\rho\rho_\mu$ is the covariant derivative, Φ is the complex charged pion field, $\rho_{\mu\nu}$ is the rho field-strength tensor, and $F_{\mu\nu}$ is the photon field strength tensor. From this Lagrangian, the matrix elements can be determined. In the calculation, the graphs involving the a_1 are neglected as the contribution from a_1 has already been taken into account in the resonance portion of the model. There are three graphs, Fig. 3, whose matrix elements are listed below:

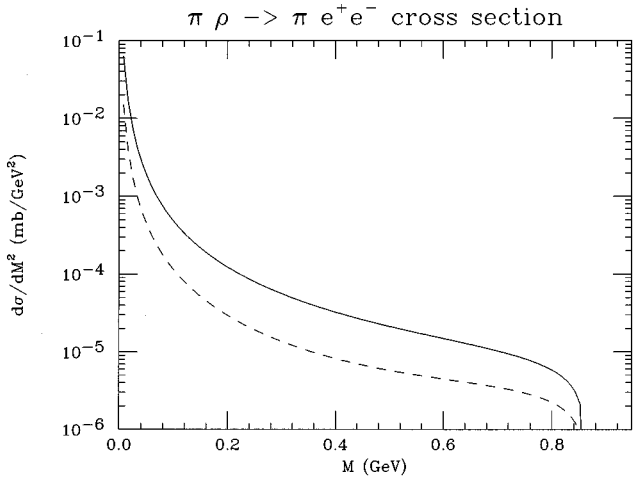

FIG. 4. Invariant mass distribution for dilepton cross section at $\sqrt{s}=1.0$ GeV. The dashed line is the distribution without form factors and the solid line includes form factors.

$$\mathcal{M}_1=\frac{g_\rho e^2}{M^2(s-m_\pi{}^2)}\epsilon^\mu(p_a)(2p_b+p_a)_\mu(2p_1+q)_\nu \times\overline{u}(p_-)\gamma^\nu\overline{v}(p_+), \tag{3.4}$$

$$\mathcal{M}_2=\frac{h_+(t)g_\rho e^2}{M^2(t-m_\rho{}^2)}\epsilon^\mu(p_a)[Y_{\mu\nu}{}^\alpha](p_b+p_1)_\mu \times\overline{u}(p_-)\gamma^\nu\overline{v}(p_+), \tag{3.5}$$

$$\mathcal{M}_3=\frac{g_\rho e^2}{M^2}\epsilon^\mu(p_a)[X_{\mu\nu}]\overline{u}(p_-)\gamma^\nu\overline{v}(p_+), \tag{3.6}$$

where $X_{\mu\nu}=ag_{\mu\nu}+b(p_{1\mu}p_{b\nu}+p_{b\mu}p_{1\nu})+c(p_{b\mu}p_{b\nu}+p_{1\mu}p_{1\nu})$ and $Y_{\mu\nu}{}^\alpha=(2p_a-q)_\nu g_{\mu\alpha}-(p_a-q)_\mu g_{\mu\alpha}-p_{a\alpha}g_{\mu\nu}$.

In the t-channel matrix element, a form factor, $h_+(t)=(\Lambda^2-m^2)/(\Lambda^2-t)$, appears to account for the finite size of the mesons. Its presence breaks gauge invariance. In order to completely restore gauge invariance, other terms must be added to the four point diagram $\mathcal{M}_3$: $a=-1$; $b=c=[h_+(t)-1]/(p_b\cdot q+p_1\cdot q)$. The parameters Λ and m are set to 1.8 GeV and m_ρ, respectively.

The absolute square $|\mathcal{M}_1+\mathcal{M}_2+\mathcal{M}_3|^2$ and $d\sigma/dM^2$ were used to Monte Carlo the three-body $\pi^\pm e^- e^+$ final state.

The invariant mass distribution, $d\sigma/dM^2$, resulting from the above matrix elements is plotted in Fig. 4. The dashed curve is the function without form factors present and the solid function has form factors included. The presence of form factors decreases the distribution as expected.

These lepton pairs are of nonresonant origin and are now added to the pairs from resonance decays.

At this point we need to address possible objections to this calculation. In a paper by Li, Ko, and Brown [3], a discussion of other effects which might explain the excess of dileptons is presented. The process in question is $\pi\rho\to\pi e^+e^-$. It is stated that the diagrams involved are the same as those needed to calculate the pion polarizabililty in

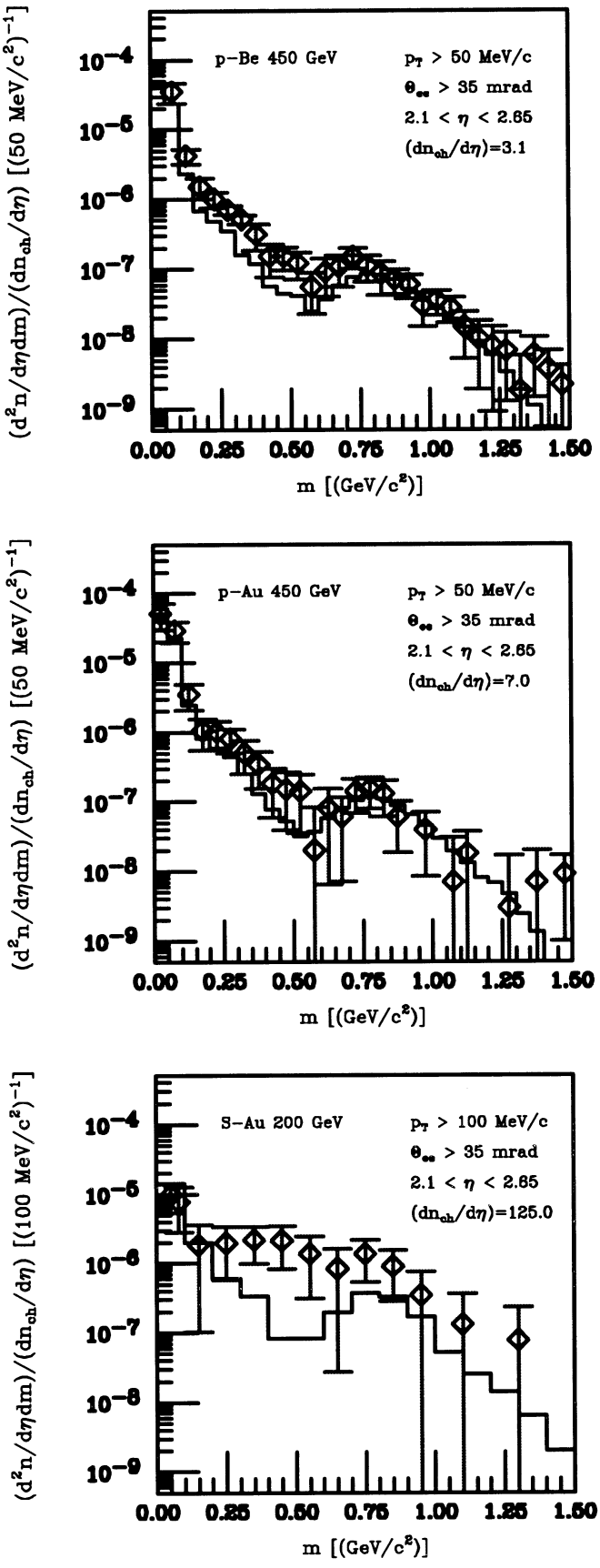

FIG. 5. Dilepton invariant mass spectra from primary scattering in the model compared to CERES data.

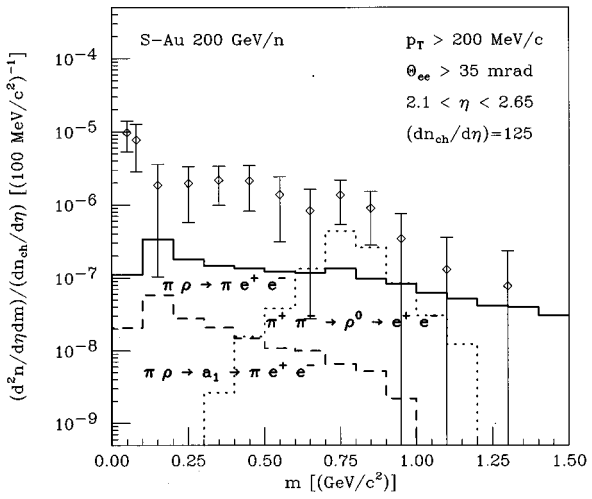

FIG. 6. Contributions from secondary scattering in S+Au collision.

the chiral limit. The work of Holstein [26] is referenced to support the claim that the only contribution to pi-rho scattering comes from the a_1 channel. The paper by Holstein shows that the diagram responsible for the bulk of the squared matrix element is canceled by a double-rho seagull, leaving only the a_1 channel. The calculation done in this paper is quite different from the one referred to by Holstein. The process described there is mediated by a pion whereas the process calculated in this paper has a rho exchange diagram [see Fig. 3]. Therefore, the processes are not the same. In addition, the Holstein paper calculates the sum of matrix elements for zero momentum transfer. This implies that any cancellation at forward angles is inferred. It is not clear in the paper by Holstein that this cancellation also occurs at nonzero momentum transfer. Furthermore, our calculations are consistent with those by Kapusta *et al.* [25].

A recent manuscript by Baier *et al.* [27] attempts a calculation similar to ours. Their results are different from ours. However, they only used the charged pion and neutral rho reaction, whereas our calculation focuses on the charged rho and neutral pion reaction. In addition, the work by Baier *et al.* contains kinematic limitiations on the lepton pair that were not made in our study.

Another possible problem occurs when comparing our results to photoproduction. Several studies have been made into photoproduction via the $\pi\rho$ entrance channel [25,21,33]. The work done by Kapusta *et al.* did not include the diagram $\pi\rho \rightarrow a_1 \rightarrow \pi\gamma$. The other works cited included the a_1 resonance in various forms. In the paper by Xiong *et al.*, the contribution from the a_1 resonance channel was comparable if not dominant to the nonresonant calculation by Kapusta, but interference effects between the a_1 diagram and the others were not taken into consideration. The study made by Song included these interference effects and showed that the contributions were comparable for one parametrization while not comparable for a different set. These results seem to contradict the results we find for dilepton production. The relative contributions between the nonresonant and resonant reactions is model dependent, but the sum is not [34,35]. Therefore, previous real photon studies are not in contradiction with our study of dilepton production.

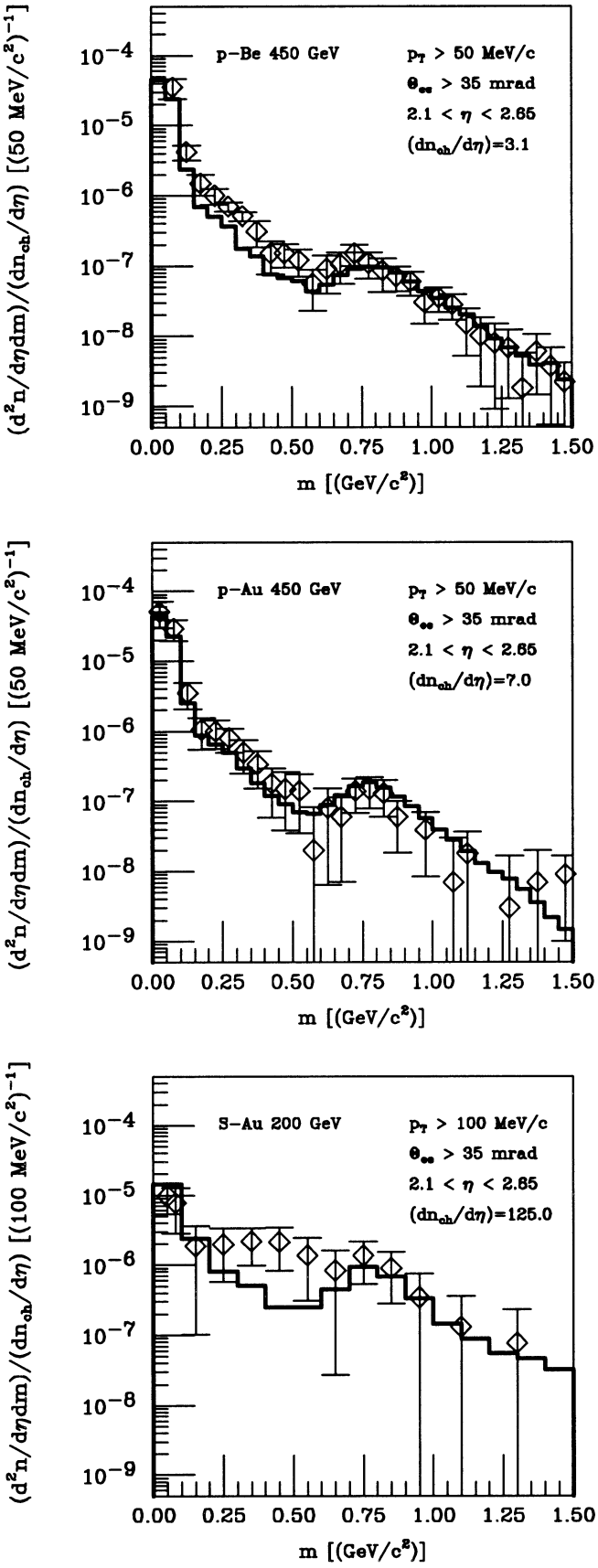

FIG. 7. Total dilepton invariant mass distributions, including primary and secondary scattering in the model as compared with CERES data.

Since the pions and rhos are scattering inside the reaction zone, their dynamics are altered by the medium. Being of bremsstrahlung type, these mechanisms are therefore susceptible to the Landau-Pomeranchuk-Migdal effect [28]. Pions and rhos involved in secondary scattering will undergo frequent multiple scatterings, and not only with other pions and rhos. Therefore, the number of dileptons produced by this scattering is reduced. The reduction factor is dependent at minimum on the invariant mass of the lepton pair as well as the mean free path of the pions and rhos. We use a reduction $1-e^{-M\lambda}$, where M is the invariant mass of the lepton pair and λ is the mean free path of the hadrons. For our purposes and level of estimation here, we set λ to some average value ~ 1 fm [29].

The total dilepton yield from our model is the sum of lepton pairs from primary plus secondary scattering. The invariant mass distributions of the dileptons from all contributions will be discussed in the last section.

IV. NORMALIZATION

In order to keep computation time low, the code was run to look at dileptons from π^0, η, η', ω, ρ^0, ϕ separately. In each run, the hadron considered was allowed to decay only into the dilepton channel; all other modes were prohibited. Technically, this is merely a way to maximize statistics. To reinstate absolute normalization, all lepton pairs counted were multiplied by the branching ratio for the process from which they came. This approximation is valid because the lepton decay mode is a comparatively rare event. We have successfully used this perturbative technique before to calculate high-energy photon production in the framework of BUU transport theory [30]. The secondary scattering resonance production was handled much the same way. All resonances produced from secondary scattering decayed exclusively into their lepton channels and were later multiplied by the appropriate branching ratio. Normalization procedures for nonresonance $\pi\rho$ scattering is somewhat different. Instead of a branching ratio from the Particle Data Group as before [31], the fraction of $\pi\rho$ events that result in lepton pairs in the final state is based on the calculated cross section for $\pi\rho\rightarrow\pi e^+e^-$ divided by the total cross section for $\pi\rho$ scattering. As a test as to whether or not the total cross section used is reasonable, we looked at the fraction of $\pi\rho$ events that result in real photon production using the same total cross section for $\pi\rho$ scattering. This fraction is comparable to the branching ratio for $a_1\rightarrow\pi\gamma$ and therefore consistent with results from other papers studying the relative contributions from the two channels [21,32,33].

V. RESULTS

The invariant mass spectra of dileptons from the primary scattering part of our model for three different systems are displayed in Fig. 5. The top two plots display lepton pairs from p+Be collisions and p+Au collisions, respectively. The lower plot shows dileptons in question from S+Au collisions. The simulation agrees with the proton-induced data and it is reassuring that our S+Au model-results are consistent with the cocktail from the CERES Collaboration [1]. Plotting against the actual S+Au data reveals a significant enhancement over predictions in the invariant mass region between 200 and 500 MeV. There is also a modest enhancement for masses above this range.

Dileptons from secondary scattering for the S+Au system in our model are shown in Fig. 6. The contribution from pion annihilation increases the distribution significantly in the rho mass region, but still leaves an excess below the rho mass. We should stress that we have taken vacuum rho properties throughout. Radiative a_1 decay contributes a minimal amount in the excess (or deficit) region, but the contribution from nonresonance $\pi\rho$ scattering provides the largest increase in the region of excess.

With the inclusion of the secondary scattering previously described, the invariant mass distributions of dileptons are shown in Fig. 7. The dilepton spectra from the proton-induced interactions are not significantly changed. This result is as expected—dileptons from the smaller systems are quantitatively described by primary hadronic decays. The proton-nucleus collisions do not create a heated nuclear medium large enough or dense enough to bring about significant collective effects. Conversely, the S+Au collision has a marked increase in lepton-pair production between an invariant mass of 200 and 500 MeV as well as a noticeable increase in the higher mass region. It is not surprising that secondary scattering becomes important in the S+Au system, as a dense nuclear medium is created during the collision.

Allowing for the shortcomings of our model, results still suggest that secondary scattering is an important but not complete explanation of the excess found in dilepton data. Inclusion of secondary scattering (1) preserves the consistency the primary scattering in our model has with proton-induced data, and (2) enhances the number of dileptons within the region of excess discovered in S+Au data. Although the contributions from pi-rho scattering cannot rule out other possible explanations for the excess electrons, our model's simplicity is attractive.

[1] G. Agakichiev *et al.*, Phys. Rev. Lett. **75**, 1272 (1995).
[2] W. Cassing, W. Ehehalt, and C. M. Ko, Phys. Lett. B **363**, 35 (1995).
[3] G. Q. Li, C. M. Ko, and G. E. Brown, Phys. Rev. Lett. **75**, 4007 (1995).
[4] C. Song, V. Koch, S. H. Lee, and C. M. Ko, Phys. Lett. B **366**, 379 (1996).
[5] R. Rapp, G. Chanfray, and J. Wambach, Phys. Rev. Lett. **76**, 368 (1996).
[6] J. Kapusta, D. Kharzeev, and L. McLerran, Phys. Rev. D **53**, 5034 (1996).
[7] A. Drees, Phys. Lett. B **388**, 380 (1996).
[8] A. Drees, Nucl. Phys. **A610**, 536c (1996).
[9] K. L. Haglin, Phys. Rev. C **53**, R2606 (1996).

[10] For first suggestions and preliminary results of the importance of this mechanisms, see, K. Haglin, Proceedings of INT/RHIC Workshop Electromagnetic Probes of Quark Gluon Plasma, 1996; Proceedings of the International Workshop on Hadrons in Dense Matter, GSI, Darmstadt, 1996.
[11] K. Geiger and B. Müller, Nucl. Phys. **A544**, 467c (1992).
[12] K. Geiger and B. Müller, Nucl. Phys. **B369**, 600 (1992).
[13] G. Kortemeyer, J. Murray, S. Pratt, K. Haglin, and W. Bauer, Phys. Rev. C **52**, 2714 (1995).
[14] G. Kortemeyer, J. Murray, S. Pratt, K. Haglin, and W. Bauer, NSCL Annual Report, 63, 1994.
[15] X. Wang and M. Gyulassy, Phys. Rev. D **44**, 3501 (1991).
[16] T. Sjöstrand, Comput. Phys. Commun. **82**, 74 (1994).
[17] A. D. Jackson and H. Boggild, Nucl. Phys. **A470**, 669 (1987).
[18] H. L. Lai, J. Botts, J. Huston, J. G. Morfin, J. F. Owens, J. Qiu, W. K. Tung, and H. Weerts, Phys. Rev. D **51**, 4763 (1995).
[19] R. Santo *et al.*, Nucl. Phys. **A566**, 61c (1994).
[20] NA35 Collaboration, M. Gazdzicki, Nucl. Phys. **590A**, 197c (1995); NA35 Collaboration, D. Röhrlich, *ibid.* **A566**, 35c (1994).
[21] L. Xiong, E. Shuryak, and G. E. Brown, Phys. Rev. D **46**, 3798 (1992).
[22] J. A. Dankowych *et al.*, Phys. Rev. Lett. **38**, 580 (1981).
[23] J. Janssen, K. Holinde, and J. Speth, Phys. Rev. C **49**, 2763 (1994).
[24] K. L. Haglin, Proceedings of the International Workshop on Soft Dilepton Production, Lawrence Berkeley National Laboratory, 1997, http://www.macdls.lbl.gov/dilepton.html
[25] J. Kapusta, P. Lichard, and D. Seibert, Phys. Rev. D **44**, 2774 (1991).
[26] B. Holstein, Comments Nucl. Part. Phys. **19**, 221 (1990).
[27] R. Baier, M. Dirks, and K. Redlich, Phys. Rev. D **55**, 4344 (1997).
[28] L. D. Landau and I. Ya. Pomeranchuk, Dokl. Akad. Nauk SSSR **92**, 535 (1953); **92**, 735 (1953).
[29] K. Haglin and S. Pratt, Phys. Lett. B **328**, 255 (1994).
[30] W. Bauer, G. F. Bertsch, W. Cassing, and U. Mosel, Phys. Rev. C **34**, 2127 (1986).
[31] Particle Data Group, L. Montanet *et al.*, Phys. Rev. D **50**, 1173 (1994).
[32] T. Csörgő, J. Zimányi, J. Bondorf, H. Heisenberg, and S. Pratt, Phys. Lett. B **241**, 301 (1990).
[33] C. Song, Phys. Rev. C **47**, 2861 (1993).
[34] J. Kapusta, private communication.
[35] C. Gale, private communication.